Methods in Molecular Biology 1008

Springer Protocols

Mark A. Williams
Tina Daviter *Editors*

Protein-Ligand Interactions

Methods and Applications

Second Edition

Humana Press

Protein-Ligand Interactions

Methods and Applications

Second Edition

Edited by

Mark A. Williams and Tina Daviter

ISMB Biophysics Centre
Institute of Structural and Molecular Biology
Birkbeck, University of London
London, United Kingdom

Humana Press

Editors
Mark A. Williams
ISMB Biophysics Centre
Institute of Structural and Molecular Biology
Birkbeck, University of London
London, United Kingdom

Tina Daviter
ISMB Biophysics Centre
Institute of Structural and Molecular Biology
Birkbeck, University of London
London, United Kingdom

ISSN 1064-3745 ISSN 1940-6029 (electronic)
ISBN 978-1-62703-397-8 ISBN 978-1-62703-398-5 (eBook)
DOI 10.1007/978-1-62703-398-5
Springer New York Heidelberg Dordrecht London

Library of Congress Control Number: 2013938157

Printed on acid-free paper

Humana Press is a brand of Springer
Springer is part of Springer Science+Business Media (www.springer.com)

Contents

Contributors

Alex Breeze • *AstraZeneca R&D, Macclesfield, UK*
Mark D. Calmiano • *Department of Medicinal Chemistry, UCB Pharma, Slough, UK*
A.W. Edith Chan • *Medicinal Chemistry, Wolfson Institute for Biomedical Research, University College London, London, UK*
Nikola Chmel • *Department of Chemistry, University of Warwick, Coventry, UK; Warwick Centre for Analytical Science, University of Warwick, Coventry, UK*
Alessio Ciulli • *College of Life Sciences, University of Dundee, Division of Biological Chemistry and Drug Discovery, The Wellcome Trust Biocentre, Scotland, UK; Department of Chemistry, University of Cambridge, Cambridge, UK*
Nicola Colclough • *AstraZeneca R&D, Macclesfield, UK*
Luminita Damian • *Microcal Products, GE Healthcare, Little Chalfont, UK*
Gareth Davies • *AstraZeneca R&D, Macclesfield, UK*
Ben Davis • *Vernalis Ltd (R&D), Great Abington, Cambridge, UK*
Tina Daviter • *ISMB Biophysics Centre, Institute of Structural and Molecular Biology, Birkbeck, University of London, London, UK*
Paul Emsley • *Structural Studies, MRC Laboratory of Molecular Biology, Cambridge, UK*
Rémi Fronzes • *Unité G5 Biologie structurale de la sécrétion bactérienne, Institut Pasteur, Paris, France*
Åsa Frostell • *GE Healthcare Bio-Sciences AB, Uppsala, Sweden*
Paul J. Gane • *Medicinal Chemistry, Wolfson Institute for Biomedical Research, University College London, London, UK*
Klaus Gerwert • *Lehrstuhl für Biophysik, Ruhr-Universität Bochum, Bochum, Germany*
Stefan Geschwindner • *AstraZeneca R&D, Mölndal, Sweden*
Geoffrey Holdgate • *AstraZeneca R&D, Macclesfield, UK*
Heiko Keller • *BIOTEC, Dresden University of Technology, Dresden, Germany*
Michael A. King • *Department of Medicinal Chemistry, UCB Pharma, Slough, UK*
Carsten Kötting • *Lehrstuhl für Biophysik, Ruhr-Universität Bochum, Bochum, Germany*
Boris Kroeplien • *Department of Medicinal Chemistry, UCB Pharma, Slough, UK*
Peter N. Lowe • *Biomolecular Interactions Consultancy, Hertford, UK*
Katherine Luby-Phelps • *Department of Cell Biology, UT Southwestern Medical School, Dallas, TX, USA*
Stephen R. Martin • *Division of Physical Biochemistry, MRC National Institute for Medical Research, London, UK*
Erick Meneses • *Department of Chemistry, McGill University, Montreal, QC, Canada*
Peter Michaely • *Department of Cell Biology, UT Southwestern Medical School, Dallas, TX, USA*
Anthony Mittermaier • *Department of Chemistry, McGill University, Montreal, QC, Canada*

Gabor Mocz • *Pacific Biosciences Research Center, University of Hawaii, Honolulu, HI, USA*
William R. Pitt • *Department of Medicinal Chemistry, UCB Pharma, Slough, UK*
Shanica N. Pompey • *Department of Cell Biology, UT Southwestern Medical School, Dallas, TX, USA*
Liliana Quintanar • *Departamento de Química, Centro de Investigación y de Estudios Avanzados, Mexico City, Mexico*
Lina Rivillas-Acevedo • *Departamento de Química, Centro de Investigación y de Estudios Avanzados, Mexico City, Mexico*
Alison Rodger • *Department of Chemistry, University of Warwick, Coventry, UK; Warwick Centre for Analytical Science, University of Warwick, Coventry, UK*
Justin A. Ross • *Queensland Institute of Medical Research, Herston, QLD, Australia*
Maria J. Schilstra • *Biological and Neural Computation Group, School of Computer Science, University of Hertfordshire, Hatfield, UK*
Petra Schwille • *Max Planck Institute of Biochemistry, Am Klopferspitz 18, Martinsried, Germany; BIOTEC, Dresden University of Technology, Dresden, Germany*
Hans Sjöbom • *GE Healthcare Bio-Sciences AB, Uppsala, Sweden*
Richard D. Taylor • *Department of Medicinal Chemistry, UCB Pharma, Slough, UK*
David Temesi • *AstraZeneca R&D, Macclesfield, UK*
Andrew P. Turnbull • *CRT Discovery Laboratories, Department of Biological Sciences, Birkbeck, University of London, London, UK*
James P. Turner • *Department of Medicinal Chemistry, UCB Pharma, Slough, UK*
Cara K. Vaughan • *Department of Biological Sciences, Institute of Structural and Molecular Biology, Birkbeck, University of London, London, UK*
Lena Vinterbäck • *GE Healthcare Bio-Sciences AB, Uppsala, Sweden*
Lara Ward • *AstraZeneca R&D, Macclesfield, UK*
Mark A. Williams • *ISMB Biophysics Centre, Institute of Structural and Molecular Biology, Birkbeck, University of London, London, UK*
Remigiusz Worch • *Institute of Physics, Polish Academy of Sciences, Warsaw, Poland; BIOTEC, Dresden University of Technology, Dresden, Germany*

Chapter 10

Studying Metal Ion–Protein Interactions: Electronic Absorption, Circular Dichroism, and Electron Paramagnetic Resonance

Liliana Quintanar and Lina Rivillas-Acevedo

Abstract

Metal ions play a wide range of important functional roles in biology, and they often serve as cofactors in enzymes. Some of the metal ions that are essential for life are strongly associated with proteins, forming obligate metalloproteins, while others may bind to proteins with relatively low affinity. The spectroscopic tools presented in this chapter are suitable to study metal ion–protein interactions. Metal sites in proteins are usually low symmetry centers that differentially absorb left and right circularly polarized light. The combination of electronic absorption and circular dichroism (CD) in the UV–visible region allows the characterization of electronic transitions associated with the metal–protein complex, yielding information on the geometry and nature of the metal–ligand interactions. For paramagnetic metal centers in proteins, electron paramagnetic resonance (EPR) is a powerful tool that provides information on the chemical environment around the unpaired electron(s), as it relates to the electronic structure and geometry of the metal–protein complex. EPR can also probe interactions between the electron spin and nuclear spins in the vicinity, yielding valuable information on some metal–ligand interactions. This chapter describes each spectroscopic technique and it provides the necessary information to design and implement the study of metal ion–protein interactions by electronic absorption, CD, and EPR.

Key words Electronic absorption spectroscopy, Electronic circular dichroism, Electron paramagnetic resonance, Metalloprotein, Metal ions, Metal–protein interactions

1 Introduction

1.1 Metal Ion–Protein Interactions

Metal ions are an important part of biological systems, as living organisms use inorganic elements for many key processes. Metal ions most commonly serve as cofactors in enzymes, helping catalyze their reactions, but do take a broad range of functional roles that include the following: structural (Ca, Zn, Si), signaling (Ca), acid-base catalysis (Zn, Fe, Ni, Mn), electron transfer (Fe, Cu, Mo), and redox catalysis (Mn, V, Fe, Co, Ni, Cu, W). Some of the metal ions that are essential for life are strongly associated with proteins,

Mark A. Williams and Tina Daviter (eds.), *Protein-Ligand Interactions: Methods and Applications*, Methods in Molecular Biology, vol. 1008, DOI 10.1007/978-1-62703-398-5_10,

forming obligate metalloproteins, as in the case of the blue copper site in electron transfer proteins; while others may bind to the protein with relatively low affinity, as is the case of Ca, Mg, and Mn acting as activators of some enzymes. Common metal-donor atoms provided by protein residues include the following: nitrogen atoms of histidines, oxygen atoms of glutamate and aspartate residues, and sulfur atoms of methionines and cysteines. A comprehensive review of metal ions in biological systems can be found in (1).

The spectroscopic tools that are presented in this chapter are suitable to study transition metal ions. When a transition metal ion is coordinated by a set of ligands, as when it binds to a protein, the metal d orbitals will split in energy as a result of their interaction with the ligand orbitals (Fig. 1). The magnitude and characteristics of this ligand field effect is dependent on the geometry of the metal complex and on the strength of the metal–ligand interactions. The ligand orbitals that interact with the metal ion will be stabilized by the interaction (Fig. 1). For a more detailed description of the ligand field effect and bonding properties of transition metal complexes, the reader is referred to (2–6). When the d orbitals of a metal ion are not full (i.e., they have less than ten electrons), it is

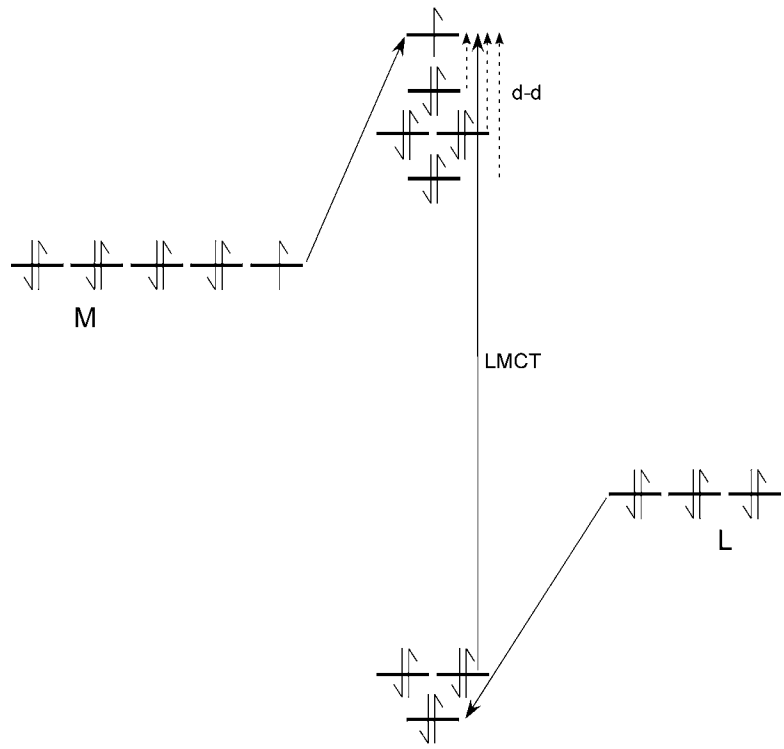

Fig. 1 Schematic molecular orbital diagram for a metal ion bound to a protein (3). Upon metal–ligand interaction, the metal d orbitals are destabilized and split in energy, while the ligand orbitals are split and stabilized. Possible ligand field (d–d) transitions are represented with *dotted arrows*, while a ligand to metal charge transfer transition (LMCT) is represented with *solid arrow*

possible to probe ligand field transitions and/or charge transfer transitions that involve ligand and metal d orbitals. Ligand field transitions refer to electronic transitions that involve orbitals with predominant metal d character, and they are often called d–d bands. Charge transfer transitions refer to electronic transitions that involve both, metal d and ligand orbitals; for example, a ligand to metal charge transfer (LMCT) is an electronic transition that originates at a ligand orbital and ends at a metal d orbital (Fig. 1). Both, ligand field and charge transfer transitions, can be probed using electronic absorption spectroscopy and circular dichroism. Finally, if the metal ion that binds to the protein of interest is paramagnetic, i.e., it has one or more unpaired electrons, then the metal–protein complex can be studied by electron paramagnetic resonance. The following sections introduce the theoretical framework for these spectroscopic tools, as inspired by their presentation in refs (7, 11).

1.2 Electronic Absorption Spectroscopy

Electronic absorption spectroscopy in the UV–visible region is a very useful, convenient and readily available technique that allows electronic transitions that occur between the ground state (Ψ_g) and an excited state (Ψ_e) of a molecule to be probed (Fig. 2); in this case the metal–protein complex. The probability of a transition due to the interaction of a photon with an electron of the metal complex is theoretically expressed through the transition moment operator $\hat{M}$. For UV–visible absorption spectroscopy, the dominant term of the transition moment operator is the electric dipole; and thus, the oscillator strength (f_{osc}) associated to an electronic transition (integrated intensity under the absorption band, Fig. 2) depends on the integral (7):

$$\int \Psi_g \hat{M}_{\text{electric dipole}} \Psi_e \, d\tau. \tag{1}$$

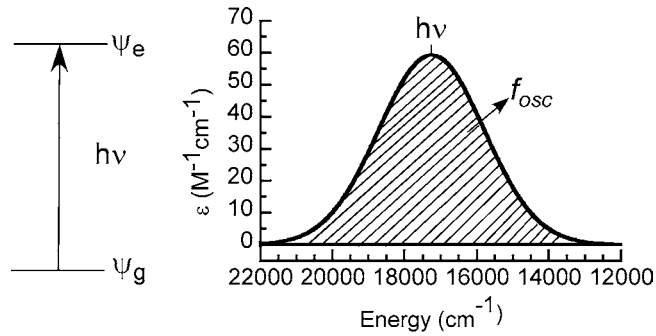

Fig. 2 Schematic diagram for an electronic transition that occurs between the ground state (Ψ_g) and an excited state (Ψ_e) of a molecule, and leads to a Gaussian-shaped absorption band (7, 11). The oscillator strength (f_{osc}) associated to the electronic transition corresponds to the integrated intensity under the absorption band, and relates to the integral in Eq. 1

If this integral is different from zero, the transition is electric dipole "allowed" and will be observed in the absorption spectrum with high intensity. If this integral is zero the electronic transition is electric dipole "forbidden"; however, this does not necessarily mean that the transition will not be observed. An electric dipole "forbidden" transition can gain intensity by several mechanisms, such as spin–orbit coupling and vibronic coupling, as discussed in refs (7–9). Thus, an electric dipole forbidden transition may be observed in the absorption spectrum, but with much lower intensity than an electric dipole allowed transition. Experimentally, an absorption band is characterized by its molar extinction coefficient (ε in M^{-1} cm^{-1}), which relates absorption intensity (A) at a given wavelength to the molar concentration (C) of the absorbing molecule through the Lambert–Beer law:

$$A = \varepsilon C l, \tag{2}$$

where l is the optical path length. The molar extinction coefficient is energy dependent with a maximum value at the energy that corresponds to the energy difference between the ground and excited states, as shown in Fig. 2.

As mentioned before, a metal complex can display ligand field (d–d) transitions and/or charge transfer transitions (Fig. 1). For metal–protein complexes, d–d transitions are usually electric dipole forbidden, and thus display small or no intensity at all. On the other hand, charge transfer transitions tend to be electric dipole allowed and they display high intensity in the absorption spectrum. From Fig. 1, it becomes evident that d–d transitions will appear at relatively lower energy, as compared to LMCT transitions. Thus, in general, in the absorption spectrum of a metal–protein complex, d–d transitions can be readily identified as they would appear in the lower energy region of the spectrum and would generally have small ε values; while LMCT transitions appear at higher energy values and have relatively high absorption intensity (*see* **Note 1**).

1.3 Electronic Circular Dichroism

Electronic circular dichroism (CD) is a widely used technique to probe the secondary structure of a protein, as discussed in Chapter 8. However, it can also be used to study electronic transitions in a metal complex that occur in the UV–visible region. CD spectroscopy uses a circularly polarized (CP) light beam, which has two components: left (L) and right (R) CP light. If a chiral molecule is exposed to CP light, its interaction with the left CP component will be different from its interaction with the right CP component, and therefore, the amount of left CP light absorbed (ε_L) by a chiral molecule will be different from its absorption of right CP light (ε_R). In a CD experiment, the difference in absorption of the two components (ε_L and ε_R) related to a given electronic transition is measured. Experimentally, a CD signal is characterized by the difference in absorption of LCP and RCP components of light

($\Delta A = A_L - A_R$); most CD instruments report this difference in ellipticity ($\theta = 32.98\ \Delta A$) in degrees. Thus, ellipticity relates to the molar concentration (C) of the absorbing chiral molecule and the difference in molar extinction coefficients for the LCP and RCP components ($\Delta\varepsilon = \varepsilon_L - \varepsilon_R$ in $M^{-1}\ cm^{-1}$) as follows:

$$\theta = 32.98 \Delta\varepsilon C l, \tag{3}$$

where l is the optical path length.

The dominant terms of the transition moment operator in UV–visible CD spectroscopy are the electric dipole ($\hat{M}_{\text{electric dipole}}$) and magnetic dipole ($\hat{M}_{\text{magnetic dipole}}$) components. The parameter that relates to the integrated area under a CD signal (Fig. 3) is the rotational strength (R), which for a given $\Psi_g \rightarrow \Psi_e$ transition, depends on the integrals (7):

$$\int \Psi_g \hat{M}_{\text{electric dipole}} \Psi_e \, d\tau \int \Psi_g \hat{M}_{\text{magnetic dipole}} \Psi_e \, d\tau. \tag{4}$$

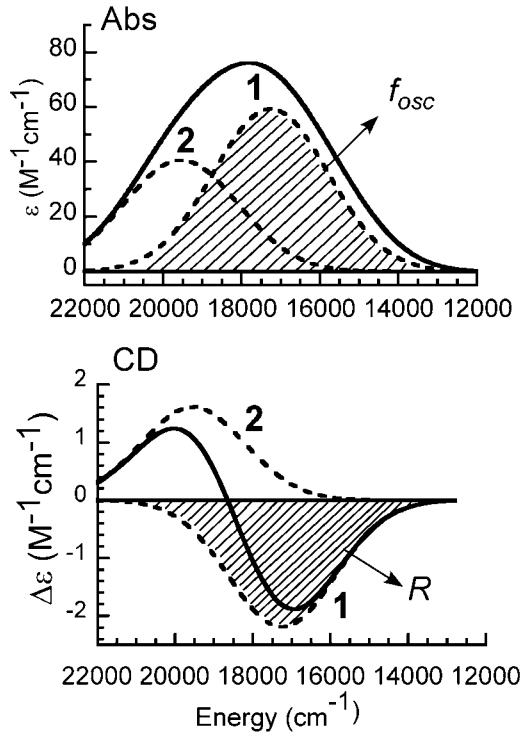

Fig. 3 Schematic diagram for two electronic transitions that are close in energy and give rise to two overlapping Gaussian-shaped absorption bands (*top*, 1 and 2). In this hypothetical case, the deconvolution of these two bands in the corresponding circular dichroism spectrum (*bottom*) is facilitated because the $\Delta\varepsilon$ for transition1 is negative, while $\Delta\varepsilon$ for transition 2 is positive. The physical parameter that relates to the integrated area under a CD signal is the rotational strength (R), which is proportional to the integral in Eq. 4 (7)

Thus, if both integrals in Eq. 4 are different from zero, the electronic transition is electric dipole and magnetic dipole allowed and it will be observed in the CD spectrum with high intensity. As in absorption, an electric dipole and/or magnetic dipole forbidden transition may be observed in the CD spectrum, as there are several mechanisms by which a forbidden transition can gain intensity (7–11).

Provided that a metal complex is chiral, as most metal–protein complexes are, CD spectroscopy can be used to probe the same electronic transitions that are probed by electronic absorption. In fact, it is quite useful to collect both absorption and CD spectra for a given metal–protein complex. Because signals observed in a CD spectrum can be positive or negative, depending on the difference $\Delta\varepsilon = \varepsilon_L - \varepsilon_R$, the overlap of two transitions in an absorption spectrum can often be more easily distinguished/deconvoluted in a CD spectrum (Fig. 3). Moreover, ligand field transitions are usually electric dipole forbidden, but magnetic dipole allowed, and thus, they gain intensity in a CD spectrum, as compared to the corresponding absorption spectrum. Thus, the ratio of the intensities displayed by a given electronic transition in CD and absorption: $\Delta\varepsilon/\varepsilon$, often called the Kuhn anisotropy factor, provides information about the type of transition. Generally, ligand field transitions display larger Kuhn anisotropy factors as compared to charge transfer transitions (7).

1.4 Electron Paramagnetic Resonance

Electron paramagnetic resonance (EPR), also called electron spin resonance (ESR), is a spectroscopic technique that allows the study of molecules with unpaired electrons. Several transition metal ions are paramagnetic, and thus, their complexes with proteins can be studied by EPR. Considering the simplest case, where a molecule has one unpaired electron, the interaction of the electron spin with the magnetic field will lead to the splitting of the spin sublevels $m_s = \pm 1/2$ of each energy state; this is called the Zeeman effect (Fig. 4). The relative energy of a particular spin sublevel m_s depends on the magnitude of the magnetic field applied to the sample (H), as given by

$$E = m_s g \beta H, \tag{5}$$

where β is the Bohr magneton and g is the g-factor or g-value. In a typical continuous wave EPR experiment, a sample is placed in a cavity and is irradiated by microwaves with a fixed frequency (υ). At the same time, a swept external magnetic field is applied to the sample, with steadily increasing field strength. When the energy difference of the Zeeman splitting between the two spin sublevels is equal to the fixed microwave energy ($h\upsilon$), the resonance condition in Eq. 6 is met, absorption of microwaves occurs and an EPR signal is detected (12, 13).

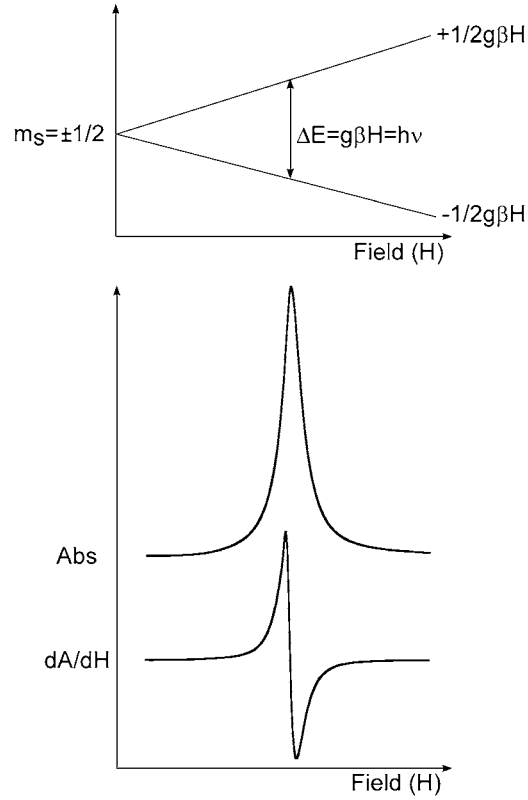

Fig. 4 Zeeman effect and the EPR experiment for a spin = 1/2 species (7, 12). The spin sublevels $m_s = \pm 1/2$ split in energy as a function of magnetic field strength (*H*) (*top*). When their energy splitting ($g\beta H$) is equal to the energy of the incident microwaves ($h\nu$), absorption of microwaves is observed. EPR spectra are displayed as the derivative of microwave absorption as a function of magnetic field (d*A*/d*H*)

$$\Delta E = g\beta H = h\nu. \tag{6}$$

EPR signals are detected by a phase sensitive detection technique, and as a result, they are usually reported as the first derivative of the microwave absorption spectrum (dA/dH) for enhanced resolution (Fig. 4). This implies that the magnetic field at which the resonance condition is achieved corresponds to the point where $dA/dH = 0$, and the peak-to-peak distance corresponds to the signal width.

Using Eq. 6, the g value associated to a paramagnetic species can be determined from the magnetic field at which the EPR signal is observed. The g-value is indicative of the chemical environment around the electron spin. For most spin = 1/2 molecules, such as free radicals, the g-value is approximately equal to 2.0023; however, for transition metal ions with one unpaired electron the g value can have small deviations from 2 due to spin–orbit coupling

(*see* **Note 2**). On the other hand, transitions metal complexes with spin $>1/2$ can have g values that deviate greatly from 2 due to zero-field splitting (*see* **Note 2**). While metalloproteins with Cu(II), V(IV), low spin Co(II), Ni(III) or Mo(V) present g values around 2, other metal sites in proteins with Mn(II), Fe(II), Fe(III), or high spin Co(II) present EPR signals with a wider range of g values (1.5–10) (7, 11, 12). A comprehensive classification of the EPR properties of metal ions found in biological systems is presented in ref. 12.

It is important to note that, as much as the chemical environment around the unpaired electron can be anisotropic, g-values may be anisotropic. This means that the magnitude of the Zeeman splitting depends on the relative orientation of the molecule with respect to the external magnetic field (Fig. 5). Thus, a paramagnetic molecule with rhombic symmetry, i.e., three nonequivalent axes, displays different g values: $g_z \neq g_y \neq g_x$. If the relative orientation of the molecule with respect to the external magnetic field cannot be controlled (as is the case for frozen solutions of metal–protein complexes), a distribution of microwave absorptions will be observed across a range of magnetic field values that correspond to the range of g_z to g_y to g_x. The first derivative of the absorption spectrum usually allows the signals associated to the three different g values to be resolved (Fig. 5).

Additionally, any nuclear spin, of magnitude I, in the vicinity of the unpaired electron will cause a hyperfine splitting of the EPR signal into $2I + 1$ signals. The magnitude of the hyperfine interaction with the nearby nucleus (N) is given by ${}^{N}A$, the hyperfine coupling constant, and it is of anisotropic nature. Several transition metal ions have nuclear spins that couple with their unpaired electrons; Cu^{2+} and V^{4+} display EPR signals split by metal hyperfine couplings due to their nuclear spins: $I = 3/2$ and $I = 7/2$, respectively (Fig. 6). A detailed analysis of the g values and metal hyperfine couplings can provide information of the geometry of the metal–-protein complex and the nature of the ligating residues. For example, for Cu^{2+} complexes the parallel g and ${}^{Cu}A$ values are very sensitive to the nature of the equatorial ligands, and they correlate well with the type of ligating atoms in the coordination shell (14, 15). Similar correlations between EPR parameters and the nature of the coordination environment for other types of metal centers in proteins, such as heme proteins, have been reported (12, 16–18).

Beyond the metal ion, other common hyperfine interactions with nearby nuclei in metal–protein complexes are those with nitrogens ($I = 1$) and protons ($I = 1/2$). These interactions are usually weaker than metal hyperfine interactions and lead to small hyperfine coupling constants (10–20 $\times$ 10^{-4} cm^{-1} for nitrogen and <5 $\times$ 10^{-4} cm^{-1} for proton) that can sometimes be resolved in a typical EPR spectrum; however, pulsed EPR techniques like ESEEM (Electron Spin Echo Envelope Modulation) or ENDOR

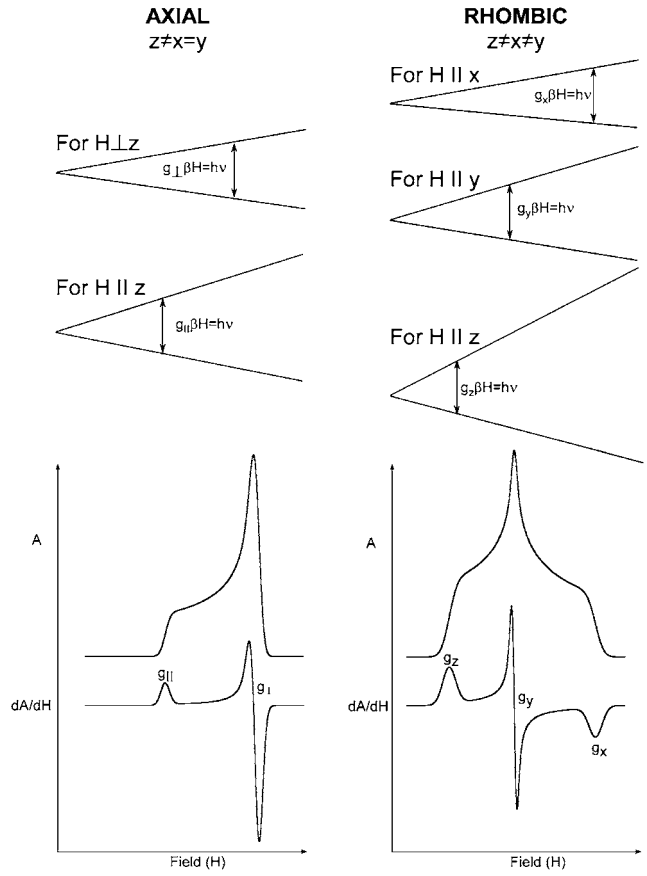

Fig. 5 Anisotropy of *g* values (7, 12). For an axial complex (*left*) with $g_z > g_y = g_x$, g_z is also called $g_{||}$ and $g_y = g_x$ correspond to $g_\perp$, and the microwave absorption spectrum displays a distribution of absorptions that range from the resonance condition for $g_{||}$ ($g_{||}\beta H = h\nu$ when the magnetic field is parallel to z), to the resonance condition for $g_\perp$ ($g_\perp\beta H = h\nu$ when the magnetic field is perpendicular to z), including all possible intermediate orientations. Thus, the EPR spectrum (d*A*/d*H*) of an axial complex will display two signals associated to the values $g_{||}$ and $g_\perp$. Similarly, for a rhombic complex (*right*) with $g_z > g_y > g_x$, a distribution of absorptions that include the three resonance conditions (for $g_z\beta H$, $g_y\beta H$, and $g_x\beta H$) will be observed

(Electron Nuclear Double Resonance) are more appropriate for an accurate measure of weak hyperfine interactions (19–21).

2 Materials

2.1 Sample Preparation

2.1.1 Water

When studying metal ion binding to proteins, it is essential to use ultra pure water with high resistivity (18 MΩ/cm). Regular distilled water may have a significant amount of metal ions that can bind to the protein under study (*see* **Note 3**).

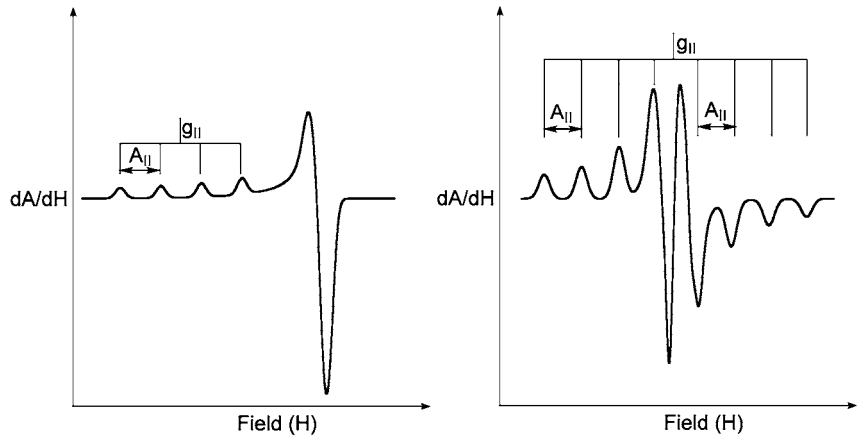

Fig. 6 EPR simulations of axial complexes of Cu^{2+} (*left*) and V^{4+} (*right*). The hyperfine interaction of the unpaired electron with the nuclear spin of ^{63}Cu and ^{65}Cu ($I = 3/2$) leads to the splitting of EPR signals into four lines, while the hyperfine interaction with the nuclear spin of ^{51}V ($I = 7/2$) leads to a splitting into eight lines. Since the metal hyperfine splitting (^{M}A where M is Cu or V) is anisotropic, and $^{M}A_{||} >> {}^{M}A_{\perp}$ in most axial complexes, the hyperfine splitting is better resolved in the parallel region of the EPR spectra

2.1.2 Buffers

It is important to select a buffer that does not bind metal ions, such as MOPS (3-(*N*-morpholino)propanesulfonic acid) or MES (2-(*N*-morpholino)ethanesulfonic acid). If a protein is in a buffer that binds metal ions, the buffer may compete with the protein for the metal ion and shift the binding equilibrium. For a complete listing of non-complexing buffers that are appropriate to use in biological systems with metal ions see ref. 22.

2.1.3 Protein Solution

The protein concentration must be such that the absorption and CD signals (particularly the d–d transitions) show reasonable intensity and a good signal-to-noise ratio; a good starting concentration can be in the range of 0.1 and 1 mM (*see* **Note 4**). Protein or peptide concentration must be accurately known, either by absorption (using the corresponding extinction coefficient), or by BCA or Bradford assays (23, 24). When the metalloprotein is analyzed by EPR at low temperatures (4–150 K), it is advisable to prepare protein samples with a cryoprotectant such as glycerol, which also helps to achieve adequate glassing (*see* **Note 5**).

2.1.4 Metal Ion Solution

If the protein will be titrated by the metal ion, the concentration of the metal ion stock solution must be as high as possible in order to avoid diluting the protein. Some metal salts are insoluble in water; in such cases, the use of a metal ion chelator may be advisable to improve solubility. Care must be taken to choose a metal chelator with a lower metal binding affinity than that of the protein under study; additionally, data analysis must consider how the

metal–protein binding equilibrium is affected by the competing chelator (25, 26).

2.2 Quartz Cells

2.2.1 Quartz Cells for Optical Measurements

For the collection of electronic absorption and CD data in the UV–Vis region, quartz cells that transmit the whole wavelength range must be used (*see* **Note 6**). Care must be taken to have the incident light beam passing through the sample, if the light is reflected or partially cut by the meniscus of the sample, the walls or base of the cell, the measured spectrum would be affected by scattered light. If the available amount of protein sample is small, semi-micro and micro quartz cells that allow data collection in very small volumes (as low as 10 μL) without decreasing the path length are commercially available. The path length of the quartz cell must be optimized in order to avoid saturation of the absorption signal (*see* **Note 4**).

2.2.2 Quartz Cells for EPR Measurements

Quartz cells must also be used for EPR experiments, as regular glass typically contains paramagnetic impurities that may interfere with the EPR signal of interest. The internal diameter of commercially available quartz tubes for EPR range from 2 to 5 mm. EPR signal intensity depends on sample concentration and on how much of the sample is inside the EPR cavity (*see* **Note 7**). Thus, the choice of internal diameter of the quartz cell depends on how much protein sample is available. Also, care must be taken to optimize the position of the quartz cell in the cavity (*see* **Note 7**).

2.3 Instrumentation

2.3.1 UV–Vis Spectrometer

There is a wide range of spectrometers commercially available, generally they are relatively inexpensive and easy-to-use. It is advisable to use one with a diode-array detector, such that the absorption spectrum can be collected from 190 to 1,100 nm at once (instead of waiting for a scan). Most UV–Vis spectrometers have two lamps: a deuterium lamp as a UV source and a tungsten lamp for the visible region. Spectrometers usually have checkup routines to make sure that the lamps are working optimally and enough light goes through the sample. If the absorption spectra are noisy, one of the first things to check is the condition of the lamps.

2.3.2 CD Spectropolarimeter

All commercially available spectropolarimeters collect CD data by scanning the wavelength and measuring CD signal at each point. Thus, it is important to check that the wavelength and CD signal intensity are calibrated (*see* **Note 8**). A flow of high purity nitrogen gas must be supplied to the lamp for at least 5 min before turning it on and as long as the lamp is on: this is to prevent the production of ozone and damage of optical components, and to displace oxygen in the sample cavity that would absorb incident light at low wavelengths. Please refer to Chapter 8 for further technical details on CD instrumentation and data collection.

2.3.3 EPR Spectrometer

The essential components of an EPR spectrometer are the following: (a) a microwave bridge that houses the microwave source and detector, (b) a resonant cavity where the sample is placed, (c) a magnet with a field controller that allows the magnetic field to be swept, and a console that performs the signal processing and controls the electronics. The microwave source can be a klystron or a Gunn diode (in newer instruments). In an EPR experiment, the microwave frequency is commonly fixed; the most widely used EPR spectrometers have a bridge that generates microwaves of ~9.5 GHz (X-band spectrometers). This frequency is useful for studying free radicals and transition metal ions using an electromagnet in the range of 0–10,000 G (Gauss = 0.0001 T). An EPR signal associated with a g value of 2 would resonate at a field of ~3,394 G at 9.5 GHz. Other microwave frequencies are commercially available for more specific applications, for example: 1 GHz (L-band), 3 GHz (S-band), 35 GHz (Q-band), and 95 GHz (W-band). EPR spectrometers with low microwave frequencies are used for in vivo detection of free radicals. Running at low microwave frequencies, such as S- and L-bands, helps resolve small hyperfine couplings; while higher frequencies (Q- and W-bands) help resolve small anisotropy of g values. It should be noted that the magnitudes of hyperfine couplings do not change when the EPR spectrum is collected at a different frequency, while the magnetic field at which the resonance condition is achieved for a given g value does change with the frequency of the microwaves used (Eq. 6).

EPR instrument calibration is important when running (or comparing) samples in different laboratories, particularly for quantitative EPR studies. The modulation amplitude must be calibrated and the precision of the magnetic field that is applied to the sample must be checked too (*see* **Note 9**).

For low temperature EPR experiments, there are commercially available cryostats to collect temperature-dependent data, using liquid nitrogen (120–200 K) or liquid helium (4–100 K). Alternatively, a commercially available quartz finger dewar containing liquid nitrogen can be used to place the sample inside the cavity to collect EPR data at 77 K.

3 Methods

3.1 Choice of Parameters for Electronic Absorption and CD Data Collection

It is common to find that the absorption spectrum of a metalloprotein is dominated in the region between 190 and 300 nm by the intense electronic transitions associated to peptide bonds and aromatic residues. These signals sometimes limit the range of wavelengths where electronic transitions associated to the metal ion (i.e., d–d and charge transfer transitions) can be observed. Additionally, when an electronic transition has a high molar extinction coefficient, the absorption can become saturated, no longer follow

the Lambert–Beer law, and cause distortion of the absorption signal. For CD, high absorption can cause additional problems, as the CD signal is detected with a photo-multiplier tube (PMT), and having a very high absorption can cause high voltage and damage at the PMT. Thus, the protein concentration, optical path length, and wavelength range for collecting absorption and CD spectra must be optimized for each sample (*see* **Note 4**).

A few parameters need to be set for absorption data collection in spectrophotometers with diode arrays: wavelength range, data pitch, and integration time; collecting data with a 1 or 2 nm step and integration times of 1 s is advisable in order to get good spectral resolution. In the spectropolarimeter, the following parameters need to be set for CD data collection: bandwidth, data pitch, response time, and scanning speed. A clear discussion on how to choose these parameters to avoid CD signal distortion is presented in Chapter 8. A bandwidth of 1 nm or 2 nm, data pitch of 1 nm, response time of 1 s, and a scanning speed of 50 nm/min are suitable starting parameters for most metalloprotein samples.

For both spectroscopies, it is necessary to blank the instrument with your buffer solution. In most spectrophotometers, the blank is subtracted automatically from any sample measurement, while in spectropolarimeters, oftentimes the CD spectrum of the blank (baseline) must be collected and subtracted manually from every sample measurement.

3.2 Titration of a Protein with a Metal Ion, as Followed by Absorption and CD

An example of the titration of a prion protein fragment by Cu(II), as followed by absorption and CD spectroscopy, is shown in Fig. 7. The 0.5 mM peptide was titrated with a concentrated aqueous solution of $CuCl_2$ up to 2 equivalents of metal to peptide. The peptide solution alone has no signals in the monitored region of the spectra (12,000–42,000 cm^{-1}) (see Fig. 7a, b). In both spectra, several signals grow with the addition of Cu(II). The plots of absorption and CD signal intensities at selected wavelengths as a function of the number of equivalents of Cu(II) added (Fig. 7c, d) clearly show that there is one binding site for Cu in this peptide and that the formation of the copper-peptide complex is close to stoichiometric at these conditions. Although, it would be possible to estimate an equilibrium binding constant associated with the formation of the complex from such plots; lower concentrations of the analyte and titrations in both senses (i.e., titration of peptide with Cu and titration of Cu with peptide) would be needed to obtain a precise value (26, 27).

The data shown in Fig. 7a, b allow us to characterize the absorption and CD signals that arise upon the formation of the complex. The higher energy region of the absorption spectrum above 25,000 cm^{-1} (below 400 nm) is dominated by transitions with high ε values (~4,000 M^{-1} cm^{-1}) that can be assigned as LMCT bands (Fig. 7a). These transitions have positive signals in

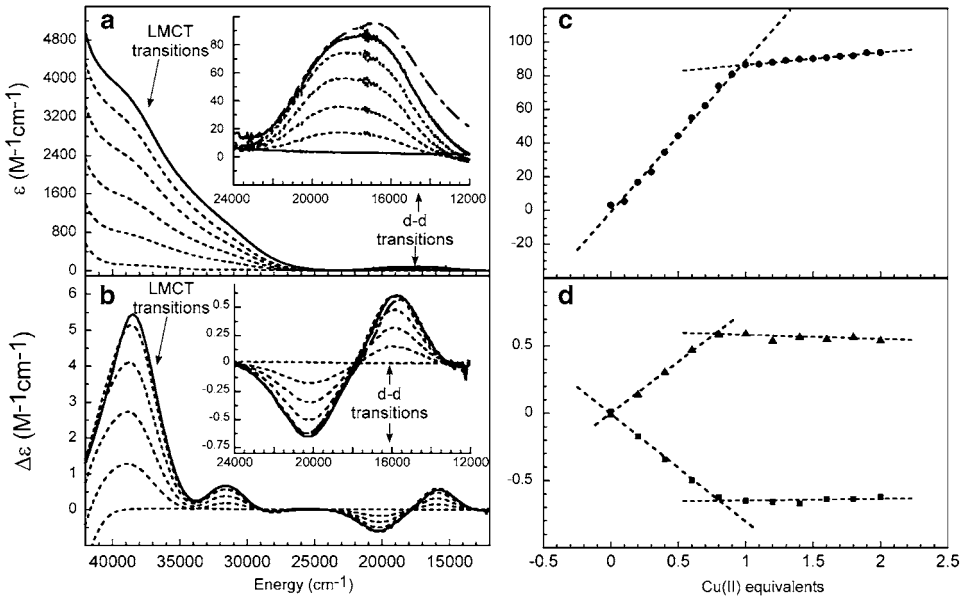

Fig. 7 Titration of the prion protein fragment KTNMKHMAGA (0.5 mM) by Cu(II), followed by absorption spectroscopy (**a**) and circular dichroism (**b**). The titration was done in 20 mM NEM buffer at pH 8.5, up to 2 equivalents of Cu(II). The spectra corresponding to titration points with <1 equivalent of Cu(II) added are shown in *dashed lines*; while spectra with 1 and 2 equivalents of metal are shown with *solid and dotted lines*, respectively. The spectral regions where d–d transitions appear are shown in the *insets*. The changes in absorption intensity at 17,760 cm^{-1} (**c**) and in CD signal intensities at 15,760 (*filled triangle*) and 20,280 cm^{-1} (*filled circle*) are shown as a function of the number of Cu(II) equivalents added (**d**). Adapted with permission from (30)

the CD spectrum (Fig. 7b). In contrast, the ligand field transitions appear at lower energy (~18,000 cm^{-1}/~550 nm) as one broad absorption signal with a very small ε value (~80 M^{-1} cm^{-1}) (Fig. 7a, inset), which is resolved in the CD spectrum as a positive band at ~16,000 cm^{-1} and a negative band at ~20,500 cm^{-1} (Fig. 7b, inset).

3.3 Absorption and CD Data Analysis

As discussed in Subheading 1.3, when absorption and CD data are available for a given metalloprotein, the electronic transitions associated with the metal complex can be better resolved and characterized. This can be done quantitatively by fitting a set of Gaussian bands to both the absorption and CD spectra, in order to deconvolve the signals that arise from each of the allowed electronic transitions of the complex, as shown in Fig. 8. The CD spectrum in Fig. 8b can be simulated with a minimum of six Gaussian bands to adequately fit all key features: four of them with a positive $\Delta\varepsilon$ and two with negative $\Delta\varepsilon$ values. The same six electronic transitions must contribute to the absorption spectrum, at the same energy as they appear in the CD spectrum, as shown in Fig. 8a. The actual height of a Gaussian band that represents a given electronic

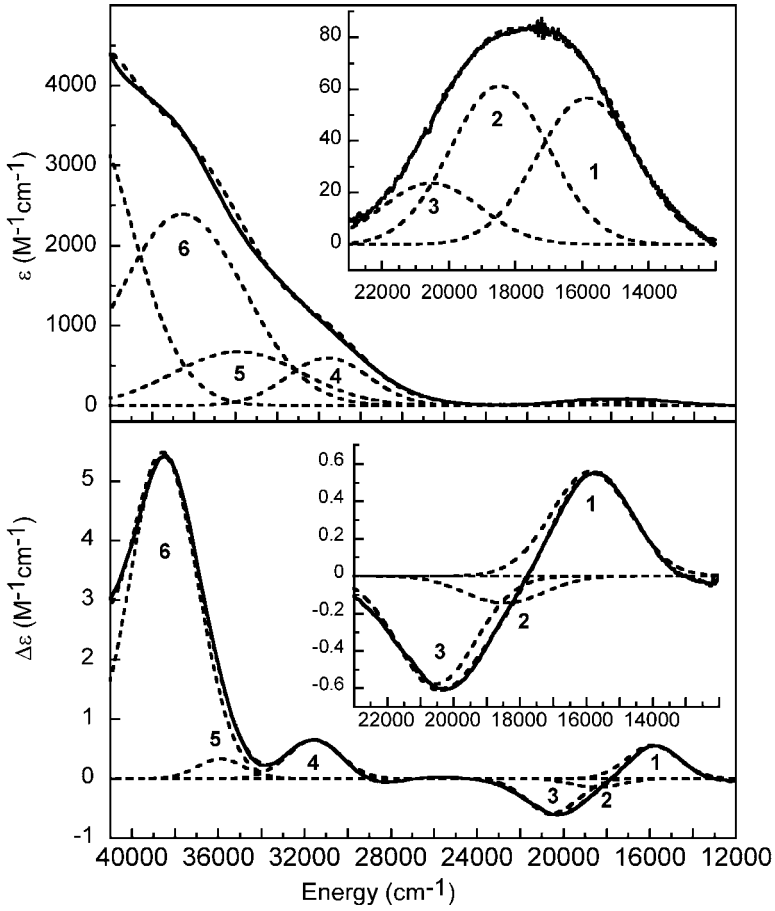

Fig. 8 Gaussian fitting/deconvolution of the UV–Vis absorption (**a**) and circular dichroism (**b**) spectra of the Cu(II)-KTNMKHMAGA complex (in 20 mM NEM buffer at pH 8.5). Experimental spectra are shown in *solid lines*, total Gaussian fit and individual Gaussian bands (with the parameters in Table 1) are shown as *dashed lines*. Adapted with permission from (30)

transition in the absorption and CD spectra corresponds to its ε and $\Delta\varepsilon$ values, respectively. The ratio of these intensities, $\Delta\varepsilon/\varepsilon$, is called the Kuhn anisotropy factor, and provides information about the nature of the transition. Gaussian bands 1–3 in Fig. 8 represent electronic transitions that can be assigned as ligand field or d–d bands, as they appear at the low energy end of the spectrum and have large Kuhn anisotropy factors (Table 1). Meanwhile, Gaussian bands 4–6 can be assigned as LMCT bands, as they appear at higher energies and have smaller Kuhn anisotropy factors (Table 1). This analysis can be carried out with any software that allows the fitting of a spectrum using the sum of several Gaussian functions.

Table 1
Parameters for the Gaussian Fits of Absorption and CD Spectra of the Cu(II)-KTNMKHMAGA complex at pH 8.5 shown in Fig. 8

Band number	Energy (cm^{-1})	ε (M^{-1} cm^{-1})	$\Delta\varepsilon$ (M^{-1} cm^{-1})	$\Delta\varepsilon/\varepsilon$ ($\times 10^{-3}$)
1 d → d	15,858	56.7	+0.561	9.90
2 d → d	18,474	61.3	−0.145	−2.36
3 d → d	20,534	23.7	−0.576	−24.3
4 N^-_{amide} → Cu CT	31,567	597	+0.654	1.10
5 N_{Im} π1 → Cu CT	35,891	675	+0.333	0.493
6 N_{Im} π2 → Cu CT	38,535	2,394	+5.42	2.27

Having precise information on the different electronic transitions that contribute to the absorption and CD spectra of a protein-bound metal ion can reveal the ligating residues of the metal site. For example, the LMCT bands 5 and 6 in Table 1 appear in a range of energies characteristic of imidazole binding to Cu(II) (28, 29), thus indicating that the metal ion in this complex is binding to a histidine. Similarly, band 4 falls in the range of energies associated with LMCT transitions from deprotonated amides to the Cu ion (29).

3.4 pH Titration of a Metal–Peptide Complex: Studying Protonation Equilibria by CD

The CD signals associated with a metal–protein complex are very sensitive to changes in coordination mode and/or changes that would modify the chirality of the complex. The CD spectrum of a Cu(II)-peptide complex changes drastically with pH in Fig. 9a. At the highest pH (pH = 9.5) the ligand field region of the spectrum (Fig. 9a, inset) shows a positive signal at ~16,000 cm^{-1} and a negative signal at ~20,500 cm^{-1}; while the LMCT bands have positive signals at ~31,500 and ~40,000 cm^{-1}. In contrast, at low pH (pH = 5.5) the ligand field region of the spectrum shows a weak negative signal at ~13,000 cm^{-1} and a positive signal at ~29,000 cm^{-1}; while the LMCT band at ~31,500 cm^{-1} changes sign. Figure 9b shows the changes in CD signal intensity as a function of pH at 15,800 and 20,800 cm^{-1}, energy values at which the changes are most dramatic. These data can be fit to a model that assumes a single protonation event, with the equation:

$$\Delta\varepsilon_{obs} = (\Delta\varepsilon_{low\ pH}[H^+] + \Delta\varepsilon_{high\ pH}K_a)/(K_a + [H^+]), \qquad (7)$$

where $\Delta\varepsilon_{obs}$ is the observed CD signal intensity at any given pH, K_a is the equilibrium constant associated to the protonation equilibrium of the Cu(II)-peptide complex, $\Delta\varepsilon_{low\ pH}$ is proportional to the CD signal intensity of the protonated form of the complex, and $\Delta\varepsilon_{high\ pH}$ to the deprotonated form. The pKa associated with the

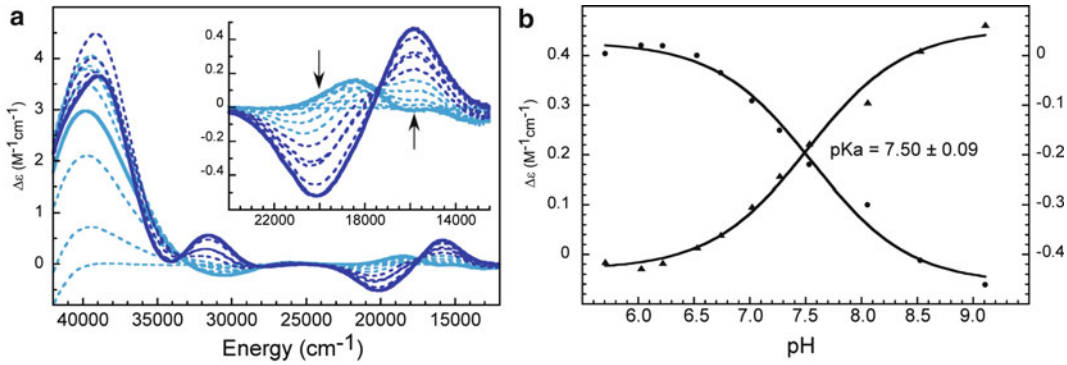

Fig. 9 pH titration of the Cu(II) complex with the prion fragment KTNMKHMAGA followed by circular dichroism. (**a**) The Cu(II)-peptide complex solutions were titrated from pH ~5.5 (*light solid line*) to pH ~9.5 (*dark solid line*); spectra for intermediate pH values are shown as *dashed lines*. The changes of CD signal intensity at 15,800 cm^{-1} (*filled triangle*) and 20,800 cm^{-1} (*filled circle*) are shown as a function of pH (**b**); the data are fit to a model (*solid lines*) that assumes a single protonation equilibrium. Reprinted with permission from (30). Copyright 2011 American Chemical Society.

protonation of the complex is 7.50 ± 0.09, as determined by the best fit of experimental data (30).

This type of analysis can be used to determine relative binding constants that relate to changes in coordination modes and/or any other effect that alters the chirality of a metal center in a protein, such as the binding of a substrate or exogenous ligand.

3.5 Getting Ready for EPR Data Collection

In an EPR spectrometer, the sample is placed in a microwave cavity, a metal box where microwaves resonate and allow the amplification of weak signals from the sample. Signal intensity depends on sample concentration and on the extent to which the microwave cavity is "filled" with the sample. For accurate quantitation of the spin concentration of the sample, the quartz cell must be filled with the sample and placed in the cavity, such that the sample occupies its full height (*see* **Note 7**).

3.5.1 Sample Positioning in the Cavity

3.5.2 Temperature

The most common EPR spectrometer uses microwaves of 9.5 GHz, corresponding to ~0.3 cm^{-1} (~0.9 cal/mol). Thus, when the resonance condition is achieved (Eq. 6) for a g value of 2 at room temperature, the Boltzmann population of spins at the lower energy spin sublevel ($m_s = -1/2$) has ~0.1 % net excess population with respect to the higher energy spin sublevel ($m_s = +1/2$). Lowering the temperature increases this difference in populations and slows down spin relaxation processes; this, in turn, increases sensitivity. Thus, the line width of the EPR spectra of most metal ions becomes sharper at low temperature. Consequently, EPR data collection on metalloproteins is usually carried out in the 4–150 K range. Reference 12 gives a general notion of optimal temperatures for the most common metal sites in proteins. It should be noted that, when the temperature is too low and the

microwave power too high, saturation of the EPR signal can occur; thus, it is important to find the optimal microwave power for the selected temperature (*see* **Note 10**). Temperature stability is very important and must be achieved before tuning the cavity and collecting EPR data. When working at low temperatures, regardless of the low temperature instrumental setup in use, care must be taken to displace the air around the quartz insert (with nitrogen or helium gas) to avoid water condensation inside the cavity. Water strongly absorbs microwaves and it can cause difficulty in tuning of the cavity.

3.5.3 Microwave Bridge

The microwave radiation source and the detector are housed in the microwave bridge. As microwaves come out of the source, they pass through a variable attenuator that can precisely control their microwave power. The higher the attenuation, the lower the microwave power. EPR signal intensity generally increases with microwave power; however, at high power levels the signal saturates, i.e., it decreases and broadens with increasing microwave power levels. The optimal microwave power for EPR data collection will depend on the nature of the sample and the chosen temperature (*see* **Note 10**). The attenuated microwaves are directed to the cavity containing the sample and are then reflected back to the microwave bridge for detection (most EPR spectrometers are reflection spectrometers in which absorption corresponds to reduction in reflected microwave intensity). Detection of reflected microwaves is generally performed with a Schottky barrier diode, which converts the microwave power into an electrical current (31). In order to optimize sensitivity and simplify quantitation, the diode should operate in its linear region (where the diode current is proportional to the square root of the microwave power); this is achieved at a corresponding optimal diode current (the actual value may vary for each microwave bridge). A small amount of microwave power, "bias," can be sent directly to the detector to ensure that total power (direct + reflected) at the detector is such that it operates at the optimal diode current. The reference microwaves are phase shifted so they are in phase with the reflected microwaves from the cavity as they combine at the detector. When tuning the cavity, the "bias" and reference phase shift must be adjusted to optimize the diode current for a range of microwave powers (range of attenuation values) that are appropriate for a specific sample (*see* **Note 10**).

3.5.4 Tuning the EPR Cavity

Microwaves are directed from the microwave bridge to the cavity via a waveguide, and they are coupled into the cavity via a hole, or "iris," which controls the amount of microwaves entering and reflecting from the cavity. Microwaves must resonate in the EPR cavity; this means that the cavity stores the microwave energy. At the resonance frequency of the cavity (*see* **Note 11**), microwaves remain inside the cavity and they are not reflected back to the

bridge. The efficiency of the cavity is indicated by a quality factor (Q), which is proportional to the ratio of microwave energy stored and microwave energy dissipated from the cavity. The larger the Q value of a cavity, the greater the sensitivity of the spectrometer (31). The process of tuning the cavity optimizes its Q value with a given sample inside. The first step to tune a cavity is to find its resonance frequency at a low microwave power (generally in the range of 2–200 nW for X-band spectrometers). Next, the reference microwave power ("bias") and phase shift must be adjusted in order to get the optimal diode current at the detector. Finally, the size of the "iris" must be adjusted such that the optimal diode current is maintained throughout the range of microwave powers that will be used for a given sample. When the magnetic field reaches the resonance condition (Eq. 6) and it drives the absorption of microwaves by the sample, the amount of microwaves reflected to the bridge change and an EPR signal is observed.

3.5.5 Setting Detection Parameters

The spectrometer console contains the electronics for phase sensitive detection, which enhances the sensitivity of an EPR spectrometer. It consists in a sinusoidal modulation of the magnetic field strength at a modulation frequency. When an EPR signal is observed, microwaves that are reflected from the cavity are amplitude modulated at the same frequency. The detector is only sensitive to signals with the same modulation frequency and phase as the field modulation, suppressing signals from noise or electrical interference. Care must be taken to choose the appropriate modulation amplitude, modulation frequency, and time constant to avoid signal distortion (31). Generally, the best approach is to use an amplitude for the field modulation approximately equal to the width of the EPR signals (intensity increases with the modulation amplitude, but if the latter is larger than the line-width, the signal becomes distorted). For the resolution of the splitting between two EPR signals (a hyperfine splitting for example), it is best to use a modulation amplitude that is smaller than the splitting. The modulation frequency should not be close to any resonant frequency in the sample. In the detection electronics there is also an electronic filter that "damps" the response to variation in the input signal, filtering out high-frequency noise. The longer the time constant for this filter, the lower the noise levels in a spectrum. However, if the time constant is too long for the rate of the magnetic field scan, the EPR signal can get distorted or even filtered out. Long time constants can be used to see weak signals, but the scan rate must be adjusted accordingly to assure that the time it takes to scan a single EPR signal is greater than the time constant. A modulation frequency of 100 kHz, modulation amplitude in the range of 2–5 G and a time constant in the range of 100–400 ms are good starting parameters for metalloproteins.

3.5.6 Magnetic Field Parameters

The magnetic field must be swept in a range such that the resonance condition (Eq. 6) is achieved and the EPR signal of interest is centered in the spectrum. Free radicals appear around a g value of 2, their signals are very sharp, and a sweep of only 50 G centered around the field corresponding to $g = 2$ (~3,394 G at X-band frequency), is appropriate. In contrast, paramagnetic metal ions can have a wide range of g values (*see* **Note 2**) and their signals are broader due to spin relaxation, so wider ranges of magnetic field may be needed (~500–6,000 G). The magnetic field scan rate is determined by the conversion time, which is the amount of time that the instrument takes to integrate the signal at a given field position. Thus, the number of data points in the field scan multiplied by the conversion time yields the total sweep time. As mentioned above, the magnetic field scan rate must be adjusted according to the optimal time constant for the EPR signal of interest. For further details on selection of EPR instrument parameters, please refer to (31).

3.6 EPR Data Analysis

3.6.1 Baseline Correction

There are several sources for background EPR signals that are not associated with a sample: signals due to oxygen from air in the cavity, dirt and dust impurities that contaminate the cavity, baseline drift due to electro-mechanical effects in the resonator, small amounts of paramagnetic impurities contained in the quartz cells used to contain the sample or the quartz inserts used in low temperature experimental set-ups. Thus, it is highly recommended to run a baseline EPR spectrum, having in the cavity everything but your sample (for example you can run the buffer solution in the same kind of quartz cell as you run your sample). The subtraction of this baseline from the sample EPR spectrum will help eliminate any background EPR signals that may appear in the spectrum but are not associated to the sample. Further digital baseline correction may be needed in order to correct for baseline drift and to have the baseline of the spectrum centered at zero in the regions where no EPR signals are observed (*see* **Note 12**); this is particularly important for comparison of experimental and simulated EPR spectra.

3.6.2 Extraction of EPR Parameters from Spectra

Often times, it is relatively easy to extract from an EPR spectrum approximate g values and even metal hyperfine splittings. Figure 10 shows the EPR spectrum of a Cu(II) complex with a prion protein fragment. It becomes evident from first inspection and comparison to the copper EPR spectrum shown in Fig. 6 that, the splitting between the lowest field positive signals corresponds to the metal hyperfine coupling associated to the parallel region of the spectrum ($^{Cu}A_{\parallel}$). In contrast to the EPR simulation shown in Fig. 6, in Fig. 10 the signals associated to $g_{\perp}$ overlap with those associated with $g_{\parallel}$, and thus, only three of the four $^{Cu}A_{\parallel}$ lines can be distinguished. From Fig. 10, one can estimate that the signal associated with $g_{\parallel}$ is centered at ~3,070 G, corresponding to a $g_{\parallel}$ ~ 2.195

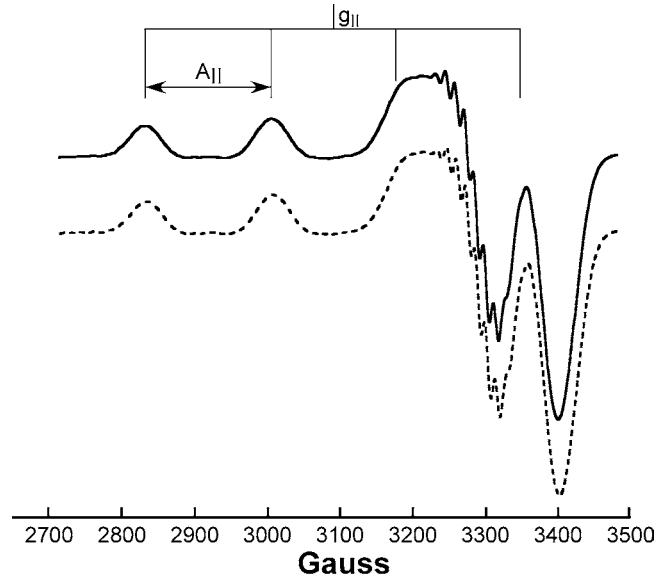

Fig. 10 Experimental X-band EPR spectrum of the Cu(II)-KTNAKHAAGA complex (*solid line*) and its EPR simulation (*dashed line*). Peptide concentration was 0.5 mM with 0.9 equivalents of Cu(II), in 20 mM NEM buffer with 50 % glycerol, at pH 8.5. The spectrum was collected in a Bruker EMX spectrometer at 150 K; microwave power = 10 mW; modulation amplitude = 5 G; modulation frequency = 100 kHz; time constant = 327 ms; conversion time = 82 ms; and microwave frequency = 9.4312 GHz. The EPR simulation was performed with the program XSophe (32), using the parameters in Table 2. Adapted with permission from (30)

(*see* **Note 11**), and that $^{Cu}A_{\|}$ is ~200 G, corresponding to ~205×10^{-4} cm^{-1} (*see* **Note 13**). This combination of $g_{\|}$ and $^{Cu}A_{\|}$ values fall in the range of parameters found for tetragonal Cu(II) complexes with four nitrogen ligands in the equatorial coordination shell (14, 15). The estimation of the $g_{\perp}$ value and the metal hyperfine in this region ($^{Cu}A_{\perp}$) is much harder to obtain due to the signal overlap and the fact that $^{Cu}A_{\perp}$ is relatively small. Additionally, the fine structure observed in the perpendicular region of the spectrum at around 3,300 G is evidence for nitrogen hyperfine coupling, indicating that the metal ion has strong coupling with its nitrogen ligands. One of the nitrogen ligands is the histidine residue, while the other three nitrogens are deprotonated amides from the backbone of the prion protein fragment, which tend to yield highly covalent Cu–N bonds, and thus, strong ^{N}A hyperfine couplings (30). Note that the participation of nitrogen donor ligands (histidine residue and deprotonated amides) can be confirmed by the presence of corresponding LMCT bands observed in absorption and CD (Subheading 3.3). This is an example of how different spectroscopic techniques can provide complementary information that help elucidate the structural features of a metal binding site in a protein.

3.6.3 EPR Spectrum Simulation

Although a lot of information can be extracted from a visual inspection of an EPR spectrum as discussed above, performing EPR simulations is needed in order to determine g values and hyperfine coupling constants more accurately, particularly when signals overlap, as is the case for the EPR spectrum presented in Fig. 10. EPR simulation programs allow the user to compare the experimental spectrum with several simulated ones with different trial parameters, until the best match is found. The best approach is to first estimate the g values and any large hyperfine couplings that can be readily identified by visual inspection. For example, in the spectrum shown in Fig. 10 the $g_{\|}$ and $^{Cu}A_{\|}$ values can be easily estimated and readily optimized in the simulation, while finding the optimal parameters for the perpendicular region and for the fine structure due to small nitrogen hyperfine couplings may take many trial and error rounds. Additionally, line widths are an important aspect of EPR signals that need to be simulated, they tend to be larger for transition metal ions as compared to organic free radicals, and they can also be anisotropic because line broadening can vary for different parts of the spectrum. Thus, the anisotropic line widths are three more parameters (L_x, L_y, L_z in Table 2) that one would like to extract from the experimental spectrum. It is recommended to start with as few parameters as possible, and progressively build more complex scenarios if needed.

Figure 10 shows the best EPR simulation attained for the experimental spectrum, using the EPR simulation program XSophe (32) and the parameters listed in Table 2. The simulation assumes that the four nitrogen ligands are nonequivalent and it considers rhombic anisotropy for all parameters, such that, at least 12 parameters contribute to the simulation of the perpendicular region of the spectrum. This level of complexity was needed in order to adequately simulate the fine structure observed in this region of the spectrum. Note that the $g_{\|}$ and $^{Cu}A_{\|}$ values determined from visual inspection of the EPR spectrum are not widely different from those found through the simulation; however, perpendicular g and metal hyperfine couplings, the number of nitrogen nuclei and their corresponding hyperfine couplings that contribute to the fine structure in the perpendicular region could not have been determined without the simulation.

3.6.4 Spin Quantitation

EPR spin quantitation can be a useful tool to determine how many metal binding sites a protein has for a particular paramagnetic metal ion, or to determine metal ion loading in a metallo-enzyme sample. EPR signal intensity increases with spin concentration; however, it can also change with other factors (amount of sample in the cavity, EPR cell diameter, microwave power, etc.). Thus, the collection of EPR data on a reference standard of a known spin concentration under the same conditions as the sample is absolutely necessary to

Table 2
EPR simulation parameters for the spectrum shown in Fig. 10

g_x	2.038
g_y	2.048
g_z	2.193
A_x	17
A_y	17
A_z	195
$^{N1}A_x$	14
$^{N1}A_y$	12
$^{N1}A_z$	12
$^{N2}A_x$	12
$^{N2}A_y$	14
$^{N2}A_z$	12
$^{N3}A_x$	19
$^{N3}A_y$	17
$^{N3}A_z$	17
$^{N4}A_x$	12
$^{N4}A_y$	14
$^{N4}A_z$	12
L_x	6
L_y	5
L_z	24

Hyperfine splittings and line-widths are given in $\times 10^{-4}$ cm^{-1}. The line shape of the signal was modeled as Gaussian, as implemented in the EPR simulation program XSophe (32)

quantitate the spin concentration. The reference must be chosen based on the nature of the sample to be spin quantitated, making sure that its concentration can be accurately determined and that it has EPR properties similar to the sample; this is particularly important for transition metal ions (31). To quantify EPR signal intensity precisely the area under the EPR absorption curve must be calculated and compared to that of the reference. It is very important to make sure that the EPR spectrum is baseline-corrected before the double integration (*see* **Note 12**), as any baseline drift would contribute to the total integral. The accuracy of EPR spin quantitation relies on controlling all the different sample and instrumental factors that affect EPR signal intensity, as discussed in detail in (12, 31).

3.7 EPR as a Probe of Metal Coordination Properties

As mentioned above, the EPR parameters associated with a protein-bound paramagnetic metal ion can provide valuable information on the coordination properties of the metal–protein complex. Thus, EPR is a powerful tool to evaluate how these coordination properties change upon a given event, such as substrate binding or a change in pH. Figure 11a shows the comparison of the EPR spectra of Cu(II) bound to a prion protein fragment at pH 8.5 and 6.5 (this is the same complex that was shown in Figure 10, and it has a protonation equilibrium with a p*K*a of 7.6 by CD) (30). The drastic changes observed by CD suggest that the structure of the complex changes upon protonation; these structural changes can be probed by EPR. From Fig. 11a, it becomes evident that the $g_{\|}$ and $^{Cu}A_{\|}$ values change significantly upon protonation of the complex: $g_{\|}$ increases from 2.193 to 2.227, while $^{Cu}A_{\|}$ decreases from 195×10^{-4} cm^{-1} to 167×10^{-4} cm^{-1}, indicating that the coordination shell of the Cu-peptide complex has changed. Specifically, the $g_{\|}$ and $^{Cu}A_{\|}$ values at pH 6.5 fall in the range of parameters found for tetragonal Cu(II) complexes with three nitrogens and one oxygen (3N1O) in the equatorial coordination shell (14, 15). This means that the coordination mode of the complex changes from 4N (having one His and three amide groups bound to the metal as described in Subheading 3.6.2) to 3N1O with one His, two amide groups and one carbonyl oxygen bound to Cu (30).

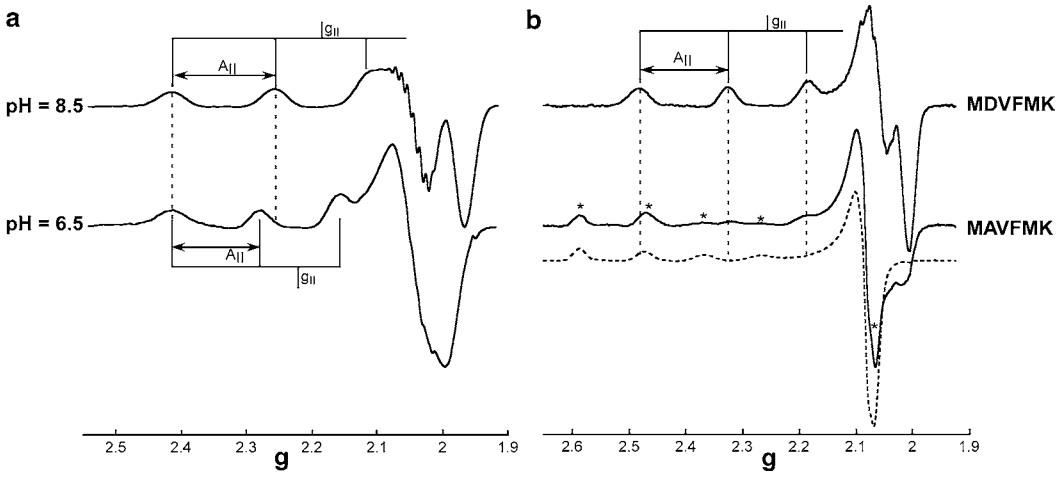

Fig. 11 Comparison of X-band EPR spectra of the Cu(II)-KTNAKHAAGA complex at pH 8.5 and 6.5 (**a**); peptide concentration was 0.5 mM with 0.9 equivalents of Cu, in 20 mM NEM and 20 mM MES buffer with 50 % glycerol. Comparison of EPR spectra of the Cu(II) complex with MDVFMK and MAVFMK peptide fragments (**b**); peptide concentration was 0.5 mM with 0.9 equivalents of Cu, in 20 mM MOPS buffer with 50 % glycerol, at pH 6.5. The EPR spectrum of free Cu(II) in the same buffer is shown as the *dashed line*, and the *asterisk* marks indicate the signals in the spectrum of the Cu(II)-MAVFMK complex that are associated with free Cu(II) in solution. Spectra were collected using the same instrument settings as in Fig. 10. Adapted with permission from (30, 33)

Additionally, the spectrum in the perpendicular region at pH 6.5 appears to be less rhombic and has less pronounced fine structure associated with nitrogen hyperfine couplings; the latter is consistent with having less nitrogen donors in the coordination shell. Combining this EPR analysis with other spectroscopic tools (absorption and CD) and electronic structure studies, models of how Cu(II) coordinates to this region of the protein can be proposed (30).

Another example for the use of EPR to probe changes in coordination properties is shown in Fig. 11b, where the EPR spectrum of Cu(II) bound to an N-terminal fragment of α-synuclein with sequence MDVFMK is compared to that of the Cu(II) complex with the peptide variant MAVFMK, to evaluate the role of the Asp2 residue in metal ion coordination. The spectrum of the Cu(II)-MDVFMK complex shows an EPR signal with $g_{\|} = 2.250$ and $^{Cu}A_{\|} = 189 \times 10^{-4}$ cm^{-1}, which are indicative of an 2N2O equatorial coordination with two nitrogens and two oxygen donors (14, 15). In contrast, the EPR spectrum of the Cu(II)-MAVFMK complex is quite different: it shows weak signals similar to those associated with Cu(II)-MDVFMK, but the spectrum is dominated by signals that correspond to free Cu(II) in solution (marked with * in Fig. 11b). In contrast to CD, where free aqueous Cu(II) ions form non-chiral complexes with water molecules and do not yield any CD signal, in EPR aqueous Cu(II) ions give rise to intense signals (dotted spectrum in Fig. 11b). The appearance of these signals in the spectrum of the Cu(II)-MAVFMK complex indicates that the affinity of Cu(II) for the peptide decreases upon the D2A substitution, and thus, under the same stoichiometric conditions, not all the metal ion is bound to the peptide. This example highlights the importance of keeping in mind that free paramagnetic metal ions (not bound to the protein) can also contribute to the EPR spectrum. These EPR results also indicate that Asp2 is one of the oxygen-based ligands and plays an important role in Cu(II) binding to this protein (33).

4 Notes

1. Exceptions to this general rule are observed in highly covalent metal sites in proteins, such as the blue copper center (34). Additionally, when the ligands have low-lying antibonding π molecular orbitals (such as N_2, CO or NO) metal to ligand charge transfer transitions (MLCT) may occur (9). Heme sites in proteins are also distinguished for their characteristic electronic spectral features, as they have low-lying empty π molecular orbitals and their highest occupied orbitals are π bonding, such that intense $\pi \rightarrow \pi^*$ transitions (called Q bands) are observed (35). When studying a metalloprotein, it is advisable

to review the relevant literature to understand the particular spectroscopic features associated to its metal ion.

2. Metal sites in proteins can be classified according to their EPR properties. Metal ions with spin $S = 1/2$, such as Cu(II), Ni (III), Ni(I) and Mo(V), present g values around 2 with small deviations (0.4 maximum) due to spin–orbit coupling, which allows for the mixing of excited ligand field states into the ground state (7, 11). The resulting spectrum can be axial or rhombic depending on the geometry of the complex. Low spin Fe(III) sites in heme proteins are $S = 1/2$ and have g values with larger deviations; a detailed analysis of their g values is a useful tool to characterize the nature of the axial ligand (12). Metal active sites in proteins with more than one paramagnetic metal ion bridged by one or more ligands can also have a total spin of 1/2, and they are described as coupled spin systems. Examples of such sites are found in iron-sulfur proteins and binuclear non-heme iron enzymes (e.g., ribonucleotide reductase or purple acid phosphatase). For example, a binuclear non-heme iron site with one Fe(II) ion (d^6) coupled to a Fe(III) center (d^5) would have a total of 11 d electrons that antiferromagnetically couple to yield a total spin of 1/2. This type of active site typically has rhombic EPR spectra with g values in the range of 1.6–2. Metal sites with $S > 1/2$, such as Mn(II), Fe (II), Fe(III), and high-spin Co(II), present zero-field splitting (zfs), which involves the energy splitting of the different m_s spin sublevels in the absence of the magnetic field, yielding g values that can greatly deviate from 2. For example, for a half-integer spin system with a total $S = 5/2$ (high-spin Fe(III) or Mn(II)), zfs will lead to an energy difference between the m_s levels $\pm 1/2$, $\pm 3/2$ and $\pm 5/2$ in the absence of the magnetic field; and each of these so called Kramers doublets will split further when the magnetic field is turned on due to the Zeeman effect. For non-Kramers or integer spin systems with an even number of unpaired electrons, the $\pm m_s$ doublets (e.g., ± 2 and ± 1 for a $S = 2$ center) are further split by zfs effects, as described in (12).
3. If the purity or high resistivity of water is questionable, sometimes it is advisable to add a chelating resin such as Chelex (a resin with high affinity for metal ions) to the buffer, in order to eliminate trace metal ions. After treatment with Chelex overnight, the resin can be easily filtered from the solution.
4. The metalloprotein sample must be concentrated enough to give a good signal-to-noise ratio, but not too concentrated that your absorption signals are saturated; absorption intensity should be ideally between 0.1 and 1.0 absorbance units, so it falls in a linear range and obeys the Lambert–Beer law (Eq. 10.2). This is particularly important for LMCT or MLCT bands, which tend to have high ε. The path length of

the cell that contains the sample will also affect the signal intensity in both, absorption and CD spectroscopy. The best choice of path length and sample concentration depends on the nature and availability of sample, and on the type of experiment; for example, you may prefer not to dilute your sample and use a cell with a shorter path length, or if you are determining binding constants, it might be desirable to keep protein concentrations low and use larger path lengths. At the optimal concentrations to observe signals associated with metal sites in metalloproteins (0.1–1 mM), the absorption of peptide bonds (between 200 and 230 nm) and aromatic residues (around 280 nm) are usually very intense, they may saturate and make it difficult or impossible to observe the signals associated with the metal site in this energy region. The choice of path length may depend on the absorption signal of interest: d–d transitions associated with a Cu(II)-protein complex are usually very weak and are best observed with a cell path length of 1 cm for metalloprotein solutions at concentration in the millimolar range; in contrast, LMCT bands that fall close to the region where the protein absorbs (200–280 nm) are best observed at shorter path lengths to avoid saturation. Usually, what works best for absorption in terms of sample concentration and cell path length would work well for CD spectroscopy. However, it is important to check in the spectropolarimeter that the voltage at the PMT detector (which is inversely proportional to the amount of light that it receives) is not too high in the selected wavelength range sweep, as high voltages may damage the PMT detector.

5. The use of glycerol for EPR sample preparation has a dual function: it serves as a cryoprotectant for the protein, and helps the sample form a disordered glass-state upon freezing. EPR cells are very fragile and tend to break easily upon freeze and thaw cycles; this effect can be minimized if the aqueous sample forms a glass. Glassing is achieved by adding 50 % glycerol to the buffer solution, and by freezing the sample very slowly. Glycerol is the most common cryoprotectant used with proteins, but it can bind metal ions; consequently, CD and absorption spectra in the presence and absence of glycerol should be compared to rule out any possible effect on the metal–protein complex. For more information on the preparation of samples for low temperature EPR experiments, including air-sensitive samples, refer to (36).
6. Commercial optical glass cells have a usable range of 334–2,500 nm. If electronic transitions below 350 nm need to be studied (typically charge transfer transitions), Spectrosil® quartz cells with a usable range of 170–2,500 nm must be used.

7. Quartz tubes for EPR measurements are available in different inner diameters (2–5 mm). The intensity of the EPR signal increases with the amount of sample that is placed in the cavity; thus, larger diameter tubes give larger signals. However, because liquid water absorbs microwaves strongly, it is advisable to use capillaries or quartz tubes with a small inner diameter with aqueous samples at room temperature. It is advisable that the EPR tube is placed far enough into the cavity, such that the sample occupies the full height of the cavity, in order to maximize the EPR signal intensity. The latter is also a requirement if you need to quantify the total spin concentration in your sample. In X-band spectrometers, the height of the cavity is 2.5 cm; thus, a volume of ~120 μL of sample in a 3 mm inner diameter quartz cell is enough to collect an EPR spectrum in optimal conditions; this volume increases to ~250 μL for cells with 4 mm inner diameter.
8. The wavelength calibration of a spectropolarimeter is performed using a neodymium crystal, which absorbs in the region from 610 to 560 nm. The data is collected with low scan speed (20 nm/min), small data pitch (0.1 nm), 0.25 s response time, and 1.0 nm band width. The maximum photomultiplier voltage must occur at 586 ± 0.8 nm. The calibration of the CD intensity is performed using an aqueous solution of 0.06 % ammonium d-10 camphor sulfonate in a 1 cm path length cell. The spectrum is collected from 350 to 250 nm with the parameters: 0.1 nm data pitch, 50 nm/min scan speed, 1.0 s response time, and 1.0 nm band width; the maximum intensity must be 190.4 ± 1 mdeg at 290.5 nm. For further details in CD instrument calibration, the reader is referred to the instrument manuals and Chapter 8.
9. Calibration of the modulation amplitude for the EPR cavity is essential in order to quantitatively compare EPR spectra run in different laboratories. This is done using a standard sample of a crystal of 2,2-diphenyl-1-picrylhydrazyl (DPPH), which gives a very narrow EPR signal. EPR spectra of the standard are collected at different modulation amplitudes; signal distortion is observed as the modulation amplitude is increased. For such a very narrow signal, the peak-to-peak width of the first derivative EPR signal is approximately equal to the peak-to-peak modulation amplitude (31). The DPPH standard is also used to check on the accuracy of the magnetic field as the signal should appear at a g value of 2.0037 ± 0.002. Although most EPR spectrometers have a probe that measures the magnetic field, the probe is usually not at the same place as the sample, and thus, there may be a small offset between the two (quartz inserts and cryostats can increase this offset). The DPPH standard can be used to calibrate the probe or DPPH may also be

used as an internal standard to determine precisely the field at the sample. Further details on EPR instrument calibration can be found in (31, 37).

10. Choice of microwave power for a given sample and setup. At low power levels, EPR signal intensity grows as the square root of the microwave power. At higher power levels, the effect of saturation occurs: the EPR signal broadens and its intensity decreases with increasing microwave power. EPR signal saturation can make it difficult to accurately measure line-widths and small hyperfine splittings. Also, to quantitate the spin concentration in a sample, both the EPR spectra of the sample and the reference, must be collected under non-saturating conditions. EPR signal saturation is most commonly observed at low temperatures. Low temperature is used to slow down spin relaxation processes, increase the net excess population of the low energy spin sublevel, and increase sensitivity; however, the combination of low temperature and high microwave power can yield an excess population of the higher energy spin sublevel, and thus to a decrease in signal intensity. The nature of spin relaxation processes depends on the nature of the sample, and EPR signal intensity depends on several factors including sample concentration, type of cavity, how much sample is placed inside the cavity, temperature and microwave power. Thus, for each sample and experimental setup that you use, a microwave power sweep must be performed in order to determine the optimal microwave power that would prevent saturation of the EPR signal. The range of optimal microwave powers is that where the signal intensity changes linearly with respect to the square root of the microwave power.
11. The microwave frequency in an X-band spectrometer is fixed at ~9.5 GHz. However, the exact value of ν at which the cavity is tuned with a sample inside may vary with its contents (sample tube, a quartz accessory for variable temperature studies, etc.). Thus, it is very important to register the exact frequency, ν, at which an EPR spectrum is run, in order to determine precisely the g value associated to a given signal. The g value associated with an EPR signal that is centered at a given magnetic field (H in gauss) can be calculated using the equation: $g = 714.46\ \nu/H$ (from substituting the Bohr magneton value and unit conversion factors in Eq. 6).
12. Sometimes, even after subtracting an EPR baseline spectrum from your sample spectrum, not all baseline drifts are corrected. Additional digital baseline correction can be carried out with many data analysis programs, using linear or polynomial functions to fit and subtract the drifting baseline; however, care must be taken not to filter out, nor "create" any EPR signals.

13. Hyperfine splittings are usually extracted from EPR spectra in magnetic field units. The conversion of A values to frequency units (cm^{-1}) as they are normally reported in the literature is given by: A (in cm^{-1}) = A (in Gauss) $\times$ $g \times 4.6686 \times 10^{-5}$, where g is the g value associated to the EPR signal that has the hyperfine splitting. A values may also be reported in MHz, the conversion between these two units is straightforward: 1 cm^{-1} = 2.9979×10^4 MHz.

Acknowledgments

L.Q. gratefully acknowledges the important scientific influence of Prof. Edward I. Solomon (Stanford University) that is clearly evidenced in this paper. This work was funded by Consejo Nacional de Ciencia y Tecnología (CONACYT grant #128255). L.R.A. has been a recipient of postdoctoral fellowships from CONACYT (grant #060366-Q and the program "Estancias Posdoctorales Vinculadas al Fortalecimiento de la Calidad del Posgrado Nacional").

References

1. Bertini I, Gray HR, Stiefel EI, Valentine JS (eds) (2007) Biological inorganic chemistry: structure and reactivity. University Science, Sausalito, CA
2. Huheey JE, Keiter EA, Keiter RL (1993) Inorganic chemistry: principles of structure and reactivity, 4th edn. HarperCollins College Publishers, New York
3. Lever ABP, Solomon EI (1999) Ligand field theory and the properties of transition metal complexes. In: Solomon EI, Lever ABP (eds) Inorganic electronic structure and spectroscopy. Wiley, New York
4. Figgis BN (1996) Introduction to ligand fields. Interscience, New York
5. Ballhausen CJ (1962) Introduction to ligand field theory. McGraw-Hill, New York
6. Ballhausen CJ, Gray HR (1964) Molecular orbital theory. Benjamin/Cummings, Reading, MA
7. Solomon EI, Hanson MA (1999) Bioinorganic spectroscopy. In: Solomon EI, Lever ABP (eds) Inorganic electronic structure and spectroscopy. Wiley, New York, pp 1–129
8. Harris DC, Bertolucci MD (1978) Symmetry and spectroscopy: an introduction to vibrational and electronic spectroscopy. Dover, New York
9. McMillin DR (2000) Electronic absorption spectroscopy. In: Que LJ (ed) Physical methods in bioinorganic chemistry. University Science, Sausalito, CA
10. Johnson MK (2000) Circular dichroism and magnetic circular dichroism. In: Que LJ (ed) Physical methods in bioinorganic chemistry. University Science, Sausalito, CA
11. Solomon EI (1984) Inorganic spectroscopy—an overview. Comments Inorg Chem 3:227–320
12. Palmer G (2000) Electron paramagnetic resonance of metalloproteins. In: Que LJ (ed) Physical methods in bioinorganic chemistry. University Science, Sausalito, CA
13. Bencini A (1999) Electron paramagnetic resonance spectroscopy. In: Solomon EI, Lever ABP (eds) Inorganic electronic structure and spectroscopy. Wiley, New York, pp 93–159
14. Peisach J, Blumberg WE (1974) Structural implications derived from the analysis of EPR spectra of natural and artificial copper proteins. Arch Biochem Biophys 165:691–708
15. Sakaguchi U, Addison AW (1979) Spectroscopic and redox studies of some copper(II) complexes with biomimetic donor atoms: implications for protein copper centers. J Chem Soc Dalton Trans 600–608
16. Cammack R, Cooper CE (1993) Electron paramagnetic resonance spectroscopy of iron complexes and iron-containing proteins. Methods Enzymol 227:353–384

17. Parish RV (1990) NMR, NQR, EPR and Mossbauer spectroscopy in inorganic chemistry. Ellis Harwood, Chichester
18. Palmer G (1979) Electron paramagnetic resonance of hemoproteins. In: Dolphin D (ed) The porphyrins. Academic, New York
19. Chasteen ND, Snetsinger PA (2000) ESEEM and ENDOR spectroscopy. In: Que LJ (ed) Physical methods in bioinorganic chemistry. University Science, Sausalito, CA
20. Deligiannakis Y, Louloudi M, Hadjiliadis N (2000) ESEEM spectroscopy as a tool to investigate the coordination environment of metal centers. Coord Chem Rev 204:1–112
21. Hoffman BM (2003) ENDOR of metalloenzymes. Acc Chem Res 36:522–529
22. Yu Q, Kandegedara A, Xu Y, Rorabacher DB (1997) Avoiding interferences from Good's buffers: a contiguous series of noncomplexing tertiary amine buffers covering the entire range of pH 3–11. Anal Biochem 253:50–56
23. Bradford MM (1976) A rapid and sensitive method for the quantitation of microgram quantities of protein utilizing the principle of protein-dye binding. Anal Biochem 72:248–254
24. Smith PK, Krohn RI, Hermanson GT, Mallia AK, Gartner FH, Provenzano MD, Fujimoto EK, Goeke NM, Olson BJ, Klenk DC (1985) Measurement of protein using bicinchoninic acid. Anal Biochem 150:76–85
25. Grossoehme NE, Spuches AM, Wilcox DE (2010) Application of isothermal titration calorimetry in bioinorganic chemistry. J Biol Inorg Chem 15:1183–1191
26. Xiao Z, Wedd AG (2010) The challenges of determining metal-protein affinities. Nat Prod Rep 27:768–789
27. Fersht A (1999) Structure and mechanism in protein science: a guide to enzyme catalysis and protein folding. WH Freeman and Company, New York
28. Bernanducci EE, Schwindinger WF, Hughey JL, Krogh-Jespersen K, Schugar HJ (1981) Electronic spectra of copper(II)-imidazole and copper(II)-pyrazole chromophores. J Am Chem Soc 103:1686–1691
29. Daniele PG, Prenesti E, Ostacoli G (1996) Ultraviolet-circular dichroism spectra for structural analysis of copper(II) complexes with aliphatic and aromatic ligands in aqueous solution. J Chem Soc Dalton Trans 3269–3275
30. Rivillas-Acevedo L, Grande-Aztatzi R, Lomelí I, García JE, Barrios E, Teloxa S, Vela A, Quintanar L (2011) Spectroscopic and electronic structure studies of copper(II) binding to His111 in the human prion protein fragment 106–115: evaluating the role of protons and methionine residues. Inorg Chem 50:1956–1972
31. Eaton GR, Eaton SS, Barr DP, Weber RT (2010) Quantitative EPR. Springer/Wien, New York
32. Hanson GR, Gates KE, Noble CJ, Griffin M, Mitchell A, Benson S (2004) XSophe-Sophe-XeprView. A computer simulation software suite (v.1.1.3) for the analysis of continuous wave EPR spectra. J Inorg Biochem 98:903–916
33. Binolfi A, Rodriguez EE, Valensin D, D'Amelio N, Ippoliti E, Obal G, Duran R, Magistrato A, Pritsch O, Zweckstetter M, Valensin G, Carloni P, Quintanar L, Griesinger C, Fernandez CO (2010) Bioinorganic chemistry of Parkinson's disease: structural determinants for the copper-mediated amyloid formation of alpha-synuclein. Inorg Chem 49:10668–10679
34. Solomon EI, Szilagyi RK, DeBeer George S, Basumallick L (2004) Electronic structures of metal sites in proteins and models: contributions to function in blue copper proteins. Chem Rev 104:419–458
35. Loew G (1999) Electronic structure of heme sites. In: Solomon EI, Lever ABP (eds) Inorganic electronic structure and spectroscopy. Wiley, New York
36. Beinert H, Orme-Johnson WH, Palmer G (1978) Special techniques for the preparation of samples for low-temperature EPR spectroscopy. Methods Enzymol 54:111–132
37. Poole CP (1983) Electron spin resonance: a comprehensive treatise on experimental techniques. Wiley, New York